Additive Manufacturing 54 (2022) 102745

Contents lists available at ScienceDirect

Additive Manufacturing

journal homepage: www.elsevier.com/locate/addma

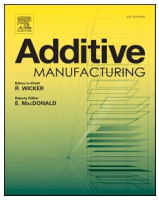

Research paper

3D reactive inkjet printing of bisphenol A-polycarbonate

Qifeng Qian [a], Jan Henk Kamps [b], Brian Price [c], Hao Gu [b], Ricky Wildman [a], Richard Hague [a], Belen Begines [a], Christopher Tuck [a,*]

[a] Centre for Additive Manufacturing, Advanced Manufacturing Building, Jubilee Campus, The University of Nottingham, NG8 1BB, United Kingdom
[b] SABIC, Plasticslaan 1, 4612 PX Bergen op Zoom, The Netherlands
[c] SABIC, 1 Lexan Lane, Mt Vernon, IN 47620, USA

ARTICLE INFO

Keywords:
Additive Manufacturing
Reactive Inkjet Printing
Polycarbonate
3D Printing
Polycondensation

ABSTRACT

Additive Manufacturing (AM) techniques have gained extensive attention recently as they are able to directly produce 3D parts utilising a layer-by-layer manner. Inkjet printing is one such technique which can produce micron-scale features but is generally constrained to liquid viscosities of less than 30 mPa·s, therefore available materials are limited. A 3D reactive inkjet printing (3DRIJP) approach to deposit low viscosity monomers and polymerise in-situ to form polymer parts is emerging. In this work, a 3DRIJP approach has been developed to fabricate bisphenol A-polycarbonate (BPA-PC) for the first time by using a low viscosity reactive ink containing monomers, catalyst and solvent. A set of processing parameters were explored and optimised including temperature of droplet formation, substrate temperature and droplet spacing to print films. With a thermal post-curing process, BPA-PC was formed successfully with a molecular weight comparable to those which were manufactured by the conventional melt transesterification process. The thermal properties were evaluated suggesting good thermal resistance characteristics. Finally, a 3D ziggurat structure was printed to demonstrate the capability to fabricate BPA-PC by an AM method, thus broadened the library of AM materials to include engineering grade polymers via 3DRJIP. This approach was innovative in both the BPA-PC material formulation and the 3DRIJP process development from traditional inkjet printing methods, where a single printable formulation of monomers for thermoplastic optical-clear BPA-PC was able to be printed using one printhead to form 3D structures.

1. Introduction

Additive Manufacturing (AM) is the collective term for manufacturing approaches allowing components to be fabricated directly from a digital model using specific materials, normally in a layer-by-layer fashion. AM technologies have rapidly grown since the mid 1980′s to become a multi-billion dollar industrial segment when the first commercial stereolithography printer emerged on the market [1]. Compared to traditional subtractive manufacturing, AM has many distinct advantages such as higher freedoms in part design, potential for lower environmental impact and higher production efficiency for lower and custom product volumes [2,3]. Today, AM has a wide range of applications in a diversity of sectors such as aerospace, automotive, construction, medicine, tissue engineering, functional prototyping, etc [4–7].

Polycarbonate (PC) is a group of polymers which contain the carbonate group within the backbone structure. Commercial PC that are available are predominantly linear aromatic thermoplastic PC which is derived from bisphenol A (BPA) as the monomer. Bisphenol-A polycarbonate (BPA-PC) is an important engineering thermoplastic which has excellent properties in optical transparency, impact and thermal resistance. Therefore, it is highly relevant to a variety of industrial applications such as civil construction, automotive and optical devices. In the context of AM, PC has attracted interest both in academia and industry. For example, selective laser sintering (SLS) using BPA-PC powders was studied [8] to investigate part morphology and mechanical properties. However, the parts suffer shrinkage and cracking due to extensive residual stress, and degradation occurs even at low laser powers. This severely compromises the physical and mechanical properties of the resultant PC parts. Material Extrusion or Fused Filament Fabrication, also known as Fused Deposition Modelling, is currently the only commercial AM technology to directly fabricate PC parts by

* Corresponding author.
E-mail address: christopher.tuck@nottingham.ac.uk (C. Tuck).

https://doi.org/10.1016/j.addma.2022.102745
Received 26 October 2021; Received in revised form 10 February 2022; Accepted 8 March 2022
Available online 12 March 2022

Table 1
Summary of physical properties of DOX25 and DMF35 at various processing temperatures required for printability assessment.

Reactive inks	Temperature (°C)	Shear viscosity (mPa s) (at 1000 s^{-1})	Surface tension (mN/m)	Density (g/cm^3)	Nozzle diameter (μm)	Z
DOX25	25	3.5	25.2	1.06	21	6.77
	35	3.3	23.7			6.96
	45	3.2	21.1			6.77
DMF35	25	2.7	35.7	1.12		10.73
	35	2.4	32.3			11.48
	45	2.1	30.4			12.73

extruding within the melt phase of a PC polymer filament. Nevertheless, extruded PC parts have several inherent drawbacks that limit application, particularly poor surface finish without post processing [9], low printing resolution [10], and a reduction in mechanical properties compared to moulded material due to process induced anisotropy [11] alongside lack of industrial scalability [12]. Therefore, to maximise the benefits of AM and PC materials an alternative AM technology is required.

Inkjet printing is a technology that produces pico-litre droplets of specific liquids or 'inks' which are deposited onto substrates selectively to form a desired pattern. Inkjet printing for 2D applications by using a polymer or nanoparticle loaded suspension is a relatively common technique particularly for graphics, printed electronics and nanocomposites [13–15] while developments in drop-on-demand (DoD) technology also enable 3D inkjet printing to fabricate objects through phase change [16] or a ultra-violet (UV) photocurable formulations [17,18]. However, though inkjet printing has inherent advantages such as micron-scale resolution, repeatability and high throughput, the narrow process window of ink viscosity (normally below 30 mPa·s) imposes a great limitation on the actual polymer materials available for this technology [19]. 3D reactive inkjet printing (3DRIJP) is an emerging AM approach that addresses this viscosity limitation by using inkjet printing to deposit multiple reactive components of materials onto targeted substrates and exploiting in-situ chemical reactions to initiate the desired material with a designed geometry [20]. With this approach, low-viscosity monomers can be processed directly rather than dissolving or melting high molecular weight polymers, thus broadening the material options for AM. Prior work has demonstrated a range of polymeric materials are possible with this method, including crosslinking two-part polydimethylsiloxane [21], gelation of hydrogel [22], polyaddition of polyurethane [23] and nylon-6 [24]. However, those materials all require two-part formulations which need 2 separate inkjet print heads to deposit droplets for in-situ mixing and polymerisation. The requirement of multi print head systems for 3DRIJP would dramatically complicate the platform design thus alter material processibility and print quality. In addition, there are no reported 3DRIJP methods that produce polycondensation-type materials available in the literature.

BPA-PC is commonly polymerised from bisphenol A (BPA) and diphenyl carbonate (DPC) in a melt transesterification process, requiring a long residence time of 2–3 h at elevated temperature of 200 °C – 300 °C. These conditions are limiting the number of comonomers which can be used and potentially lead to by-product formation[25,26]. Recently it has been demonstrated by replacing DPC with an ester-substituted activated carbonate, such as bis-(methyl salicyl) carbonate (BMSC), degradation free PC and absence of colour issues are achieved as well as a significantly increased reaction rate [27–29]. The use of BMSC to synthesise BPA-PC in a solution environment [26] also gives some insights into the material processability aspect that reactive inks can be potentially formulated. These optimised attributes have potential benefits on developing AM approaches for fabricating BPA-PC parts, such as lowering curing temperature and improving processing throughputs.

In this paper, we report a novel 3DRIJP method and materials to fabricate BPA-PC for the first time in AM. A reactive formulation was developed by mixing BPA, BMSC, an organic catalyst (i.e. tetramethyl ammonium hydroxide) and an organic solvent (i.e. 1,4-dioxane or dimethylformamide) for creating arbitrary structures by 3DRIJP. Parts were consolidated by thermal post-curing to accomplish polymerisation and enhance the molecular weight. This novel 3DRIJP method opened a new route of processing BPA-PC by AM, and eliminated the need of in-situ mixing of components on the substrate. 3DRIJP process windows were explored to print BPA-PC, and its surface profiles, chemical properties and thermal properties were characterised.

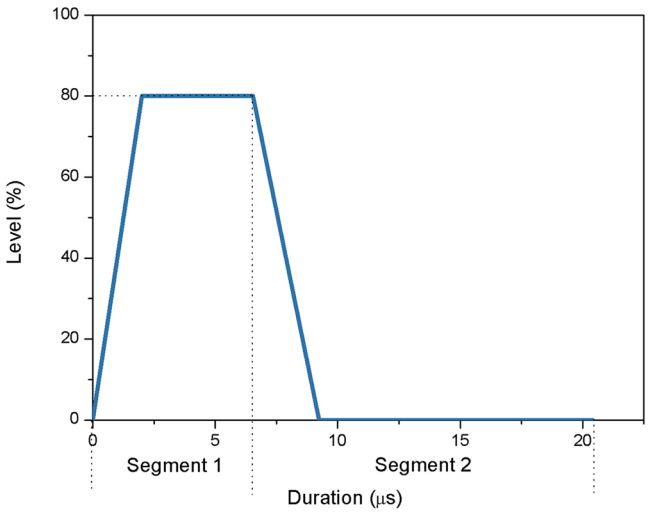

Fig. 1. The waveform pattern for jetting low viscosity fluid.

2. Results and discussions

2.1. Ink formulations and printability assessment

Firstly, two inks were formulated using 1,4-dioxane and dimethylformamide, respectively, selected for their low vapour pressure and suitability for dissolving the reactants. The sample coded DOX25 was formulated with 25 wt% of a mixture of BPA and BMSC (molar ratio 1:1.02) in 1,4-dioxane and the sample coded DMF35 was formulated with 35 wt% of a mixture of BPA and BMSC (molar ratio 1:1.02) with the procedure detailed in the Supplementary Information. The scheme of transesterification between BPA and BMSC is shown in Fig. S1. The viscosity of DOX25 and DMF35 formulations at temperatures of 25 °C, 35 °C and 45 °C were measured (Fig. S2) using a rotational rheometer. Both formulations showed Newtonian viscosity profiles. In general, they had a relatively low viscosity (<4 mPa·s) even at 45 °C. The surface tension measurement of two reactive formulations is shown in Fig. S3. As a general guide for assessing printability [30,31], the printability indicator Z (reciprocal of Ohnesorge Number) for each ink at different temperatures was calculated (Table 1). For DOX25, the Z numbers were all varying between 6.77 and 6.96 in the temperature range from 25 °C to 45 °C. The Z number is considered to indicate the printability of inks where droplets can be stably generated if $1 < Z < 10$[30]. For DMF35, the Z numbers were slightly greater than 10, and further droplet assessment was undertaken to confirm its printability.

Table 2
Jetting parameter of the waveform for jetting DOX25 and DMF35.

Waveform description			
Segment	Level (%)	Slew rate	Duration (μs)
1	80	0.36	6.528
2	0	0.22	13.888
Overall	–	–	20.416
Other jetting parameters			
		DOX25	DMF35
Maximum jetting frequency (kHz)		5	3
Jetting voltage for each nozzle(V)		23–24	25–26

A single-pulse waveform specifically designed for jetting low viscosity fluid on the Dimatix printer was used and tailored. Fig. 1 shows the waveform pattern applied in this work and Table 2 detailed all the waveform parameters. It was found that each nozzle had a different velocity profile of jetting liquid at the same jetting voltage input. Therefore, the jetting voltage for each nozzle was individually adjusted to keep the velocity of droplets at the same level.

2.2. Droplet formation and deposition

The effect of ink temperature on the droplet formation was investigated to compare and optimise the printability of both reactive inks. For DOX25 droplet formation, a single droplet without attached tails was observed at 25 °C while unmerged secondary droplets in flight with deviated jet straightness were found at 35 °C and 45 °C (Fig. S4). A similar droplet formation process was observed for DMF35, with tail retraction occurring at 200 μm travel distance at 25 °C (Fig. S5, Supplementary Information). At 35 °C and 45 °C, the tails were elongated, with no satellites observed. From these experiments, the appropriate droplet formation for both reactive inks were suggested at 25 °C without formation of satellite droplets. In order to form a continuous thin film on the substrate, the droplets must partially overlap one another, where the droplet spacing is one of the main contributors to reliable film formation. In addition, the substrate temperature plays a key role in the interaction between the droplet and the substrate affecting the film formation process and quality.

DOX25 and DMF35 were printed respectively at different substrate temperatures (50 °C, 60 °C and 70 °C for DOX25; 70 °C, 80 °C and 90 °C for DMF35) with a selected range of droplet spacing (20, 30 and 40 μm for DOX25; 15, 25 and 35 μm for the DMF35) on the microscope glass slide to investigate film formation. For DOX25, there was evidence that continuous films were obtained when the droplet spacing was fixed at 20 μm and no waviness on the surface was observed (Fig. 2). Printing was conducted using all 16 nozzles and no significant boundary interfaces were evident between the lines, which indicated that the line of the reactive mixtures did not completely dry before merging with the next one. However, crater-like pores appeared on the film surface disrupting film continuity at substrate temperatures of 70 °C. This was possibly due to incomplete wetting and bubble formation. Smaller pinholes were possibly caused by air dust contaminations. Similar film formation was obtained when the droplet spacing was 30 μm, where the wetting and bubbles led to pores on the surface. When the droplet spacing was increased to 40 μm, the continuity of the films was maintained at a surface temperature at 50°C with some pinholes existing on

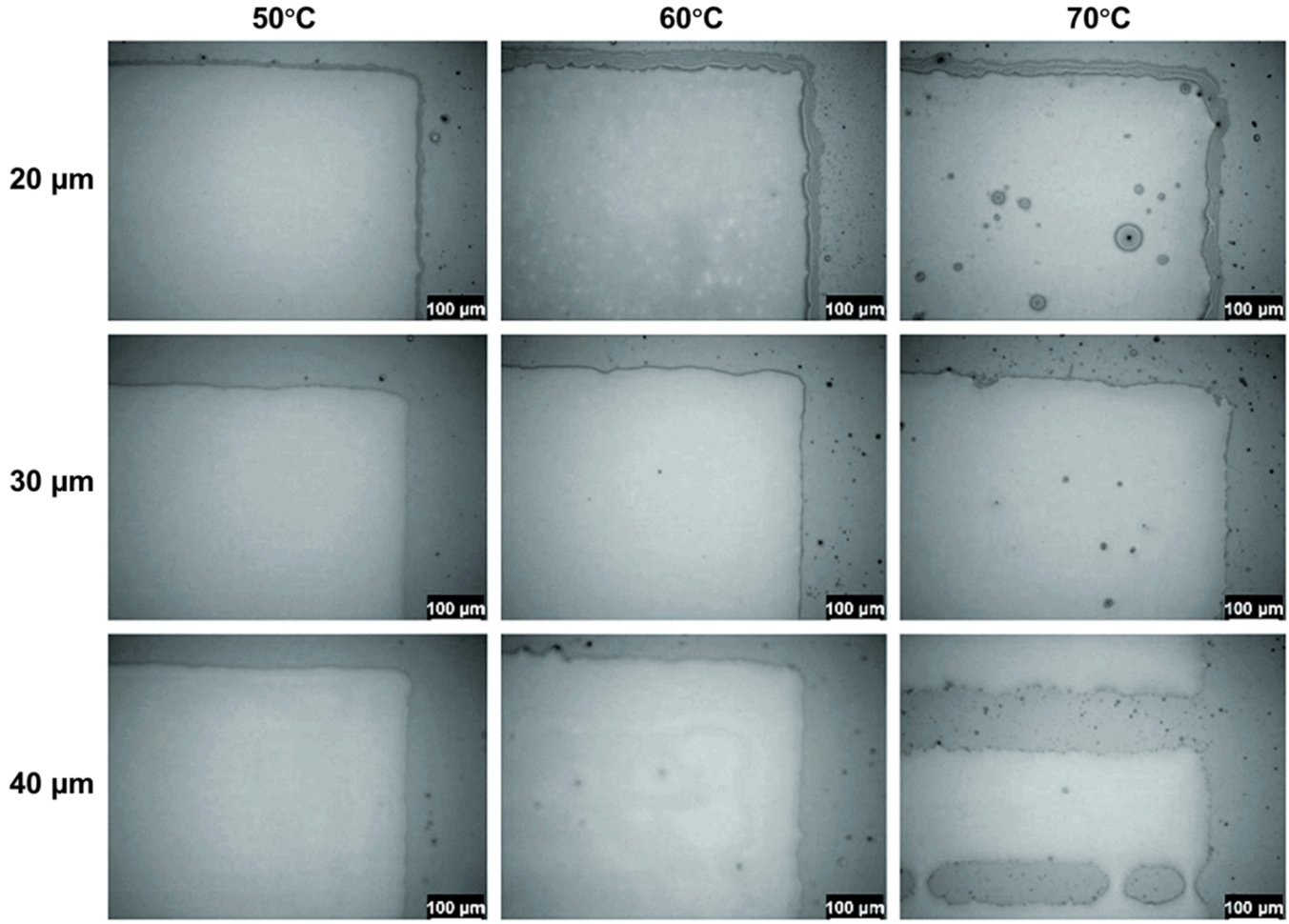

Fig. 2. The optical images for the thin films of DOX25 with different droplet spacing at various substrate temperatures.

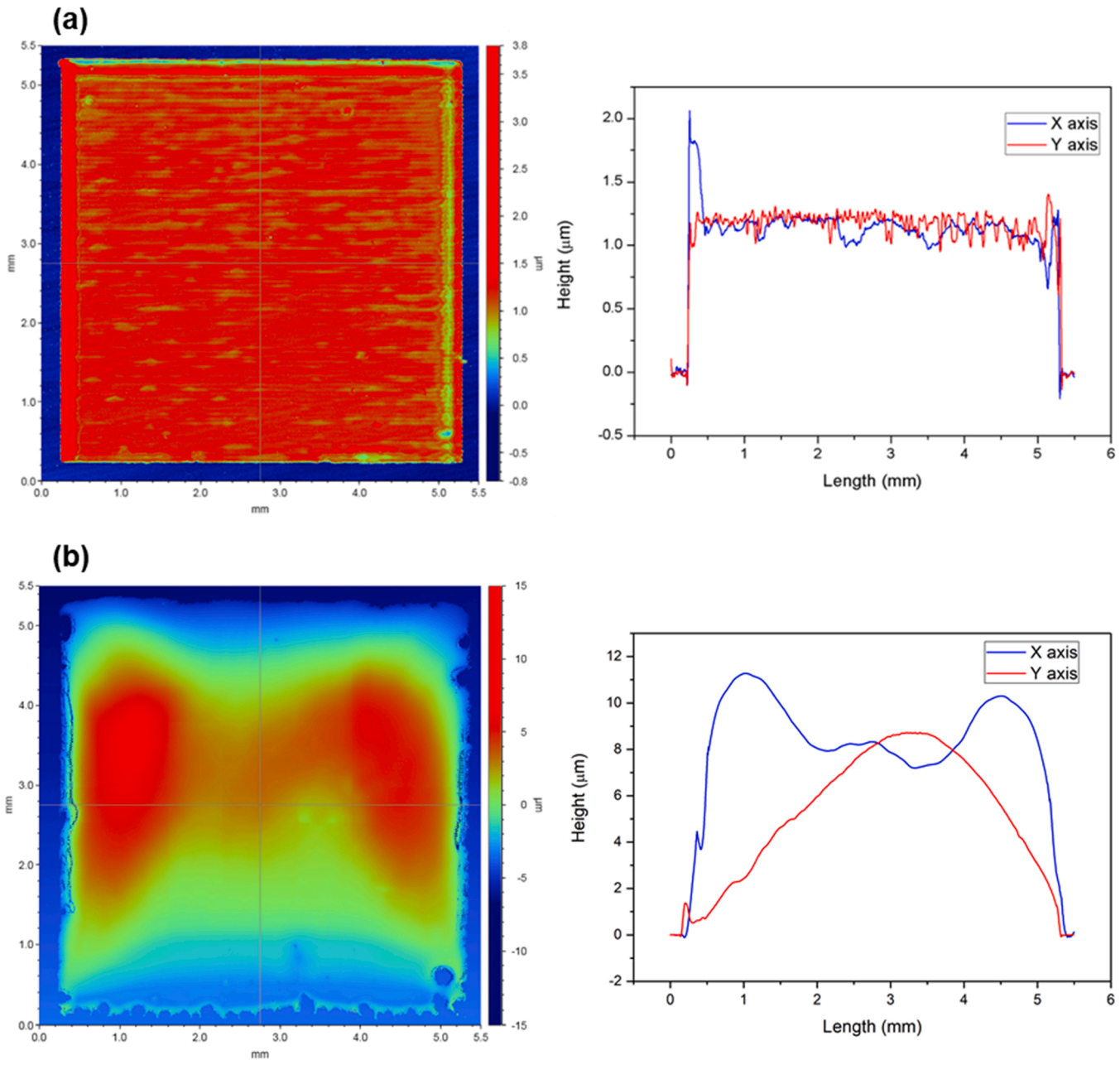

Fig. 3. The surface profiles of the thin films as printed by white light interferometer: (a) 1 layer film of DOX25 with a droplet spacing of 30 μm at 60 °C substrate temperature; (b) 1 layer film of DMF35 with a droplet spacing of 15 μm at 80 °C substrate temperature. (The X and Y profiles in the right-hand side figure pertain to the lines of crosshair in the left side figures).

the surface at 60 °C. At a substrate temperature of 70 °C, the adjacent droplets were not able to merge resulting in separate lines instead of continuous films. This was due to the effect of the jet instability and the larger droplet spacing [13]. To form homogenous films the substrate was set to 60 °C. For DMF35, continuous films were formed with a droplet spacing of 15 and 25 μm regardless of the substrate temperatures (Fig. S6, Supplementary Information).

The surface profiles of thin films were also characterised to investigate in detail their morphology and Fig. 3 shows two examples of the results. Fig. 3(a) displayed the surface morphology of a 1-layer thin film of DOX25 with a droplet spacing of 30 μm at substrate temperature of 60 °C. Note that the edges of the film did not represent the actual thickness due to the limitation of measuring slopes. The average thickness of the film was measured to be ~1.2 μm. The surface showed morphology where the boundaries between the printed threads existed, as the surface height varied more intensively in the Y axis (X axis was the printing direction). This was caused by evaporation of the solvent and the drying of the reactive mixture before the next line was printed. In contrast, the 1-layer thin film printed by DMF35 showed a different profile in Fig. 3(b). The thickness was much higher than that of the single layer of DOX25, due to a higher loading of the reactive mixture and a higher degree of swelling. No significant boundaries between the printed threads were observed which suggests a relatively low evaporation of the solvent and a well-mixed fluid before drying. However, the distribution of the reactive mixture was found to be inhomogeneous. A similar phenomenon was also reported by other work [32] where the heat flux from the substrate to the edge of the drop led to a locally enhanced solvent evaporation and the central solutes would tend to move towards the edge to replace the lost fluid. In this case, because of the slow evaporation of DMF, it was likely that the film remained fluid to

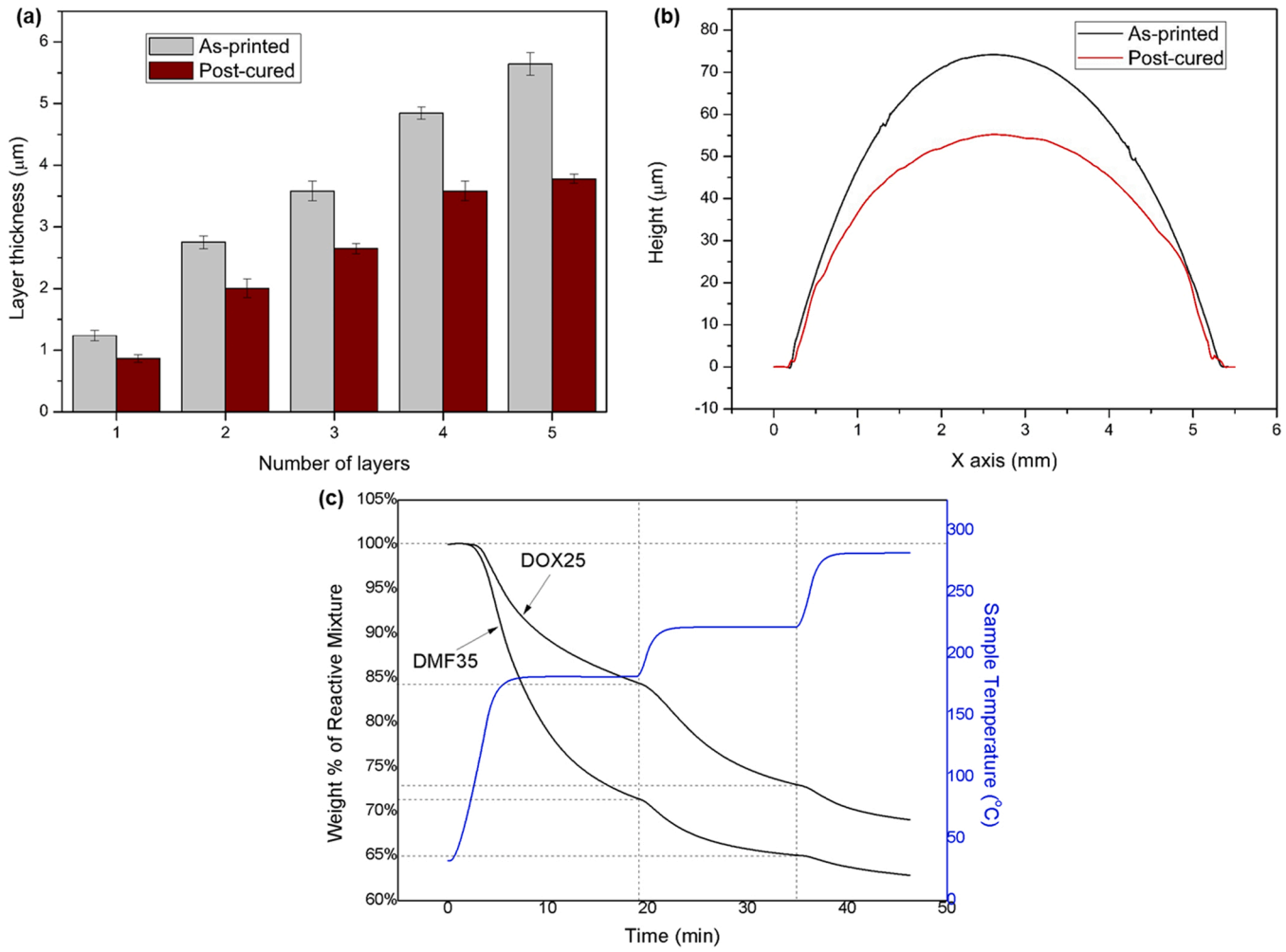

Fig. 4. (a) The comparison of the thickness of DOX25 films from 1 to 5 layers between the as-printed and the post thermal cured samples (average ± standard deviation, n = 3); (b) Surface profile analysis of 5 layers films produced by DMF35 as the comparison between the as-printed and the post-cured films; (c) A multi-stage isothermal TGA curve for the melt polymerisation process of the as-printed thin film samples.

allow the solutes to transfer to the edge. Also, it was noted that the fluid tended to transfer from the top and bottom edge of the film to the centre due to the bulk flow driven by the surface tension gradient [33].

Multi-layer reactive inks were also printed, and their surface profiles were characterised (Fig. S7, Supplementary Information). The 'dome' shape indicated a printed layer would intermix with the layer printed previously. The multi-layer overprint was able to hold its geometry in place after printing, but a contact test indicated a gel-like status of the as-printed reactive mixtures which required post-processing to further polymerise. The DSC result for the as-printed reactive mixture of DOX25 and DMF35 showed that the reactive mixture started to be 'softened' at a low temperature and then further polymerised at a higher temperature (Fig. S8). For DOX25, using a 'half Cp' method the 'T_g' of the reactive mixture was calculated to be 17°C. Then a broad endothermic peak in the heating run was observed from 139 °C which was due to the melting of the reactive mixture and the initiation of polymerisation. The molecular mobility of the reactive mixture became sufficient for the melt polymerisation from this onset temperature. In the cooling run, the peak for the melt polymerisation was not seen as the polymer would have formed. Similarly, the thermogram of as-printed DMF35 shows a T_g of 4 °C which was lower than the normal room temperature. This low T_g was due to the low molecular weight and presence of residual solvents which acted as plasticizer. The rate of melt polymerisation significantly increased from 140 °C which led to formation of BPA-PC polymer.

The as-printed multi-layer films were post cured using a stepped polymerisation method (Experimental Section, Supplementary Information). After the thermal post curing, the film thickness of DOX25 had a significant reduction which is shown in Fig. 4(a). The thickness was reduced by 25.0%, 28.6%, 27.7%, 25.0% and 32.1% for the 1–5 layers thin films respectively. This reduction was expected collectively due to the solvent evaporation, escape of methyl salicylate and the volatilisation of the monomer residue in the reactive mixture. Despite the thickness reduction, the post-cured films remained relatively flat in surface profile with sharp edge features (Fig. S9, Supplementary Information). There were pinholes on the films observed after polymerisation, which was likely to be caused by diffusion of the solvent and the volatile by-product, i.e., methyl salicylate. Compared to multi-layer films printed by DOX25, those which were printed by DMF35 showed non-flat surface profiles regardless of the as-printed or post-cured samples (Fig. S10, Supplementary Information). Typically, with 1 or 2 thin film-layers, the effect of depinning (i.e., receding of the film edge) was significant and led to a non-homogenous and therefore non-flat surface. This indicated a weak interaction between the ink and the substrate, which was attributed to a low adhesive force between the deposited droplets and the substrate surface before the solvent evaporation could complete [34]. It was reported that the contact line receding between the ink and surface was a resultant of pinning and ink-air interfacial tension [35,36]. A typical surface profile analysis of a 5 layers DMF35 film is shown Fig. 4(b) as a comparison between the as-printed and the post-cured specimen. The edges receded by ~0.3 mm after post curing.

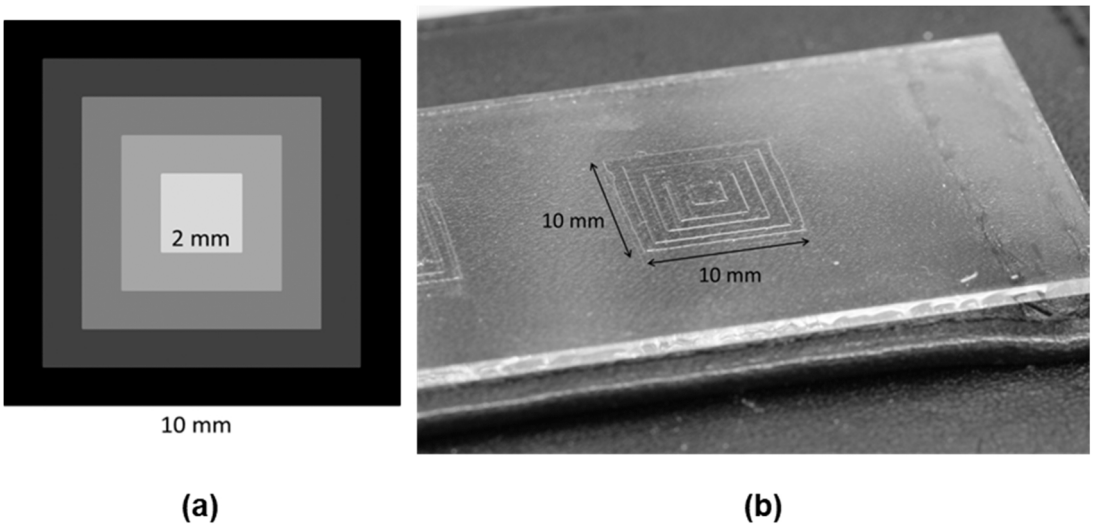

Fig. 5. The designed ziggurat structure to demonstrate the 3D printing capability of DOX25: (a) the ziggurat bitmap design for the printing pattern; (b) the printed ziggurat structure (5 layers per step, 25 layers in total).

The top of the dome sank from 73 to 54 μm, possibly resulting from the escape of the methyl salicylate. The entire surface also showed a much higher thickness when compared to those produced by DOX25, possibly due to a higher loading of reactive mixture and a larger swelling effect in DMF.

The reduction of film thickness after post-curing was further investigated by a multi-stage isothermal TGA method (Experimental Section, Supplementary Information) and the results are shown in Fig. 4(c). There was ~15.7% weight loss for the DOX25 as-printed samples during the 1st heating and the isothermal stage, which corresponded to a combination of solvent evaporation and moisture loss. During the 2nd stage, the weight loss accounted for 11.3% indicating an escape of the by-product volatiles, i.e., methyl salicylate. The completion of the melt polymerisation at the final isothermal stage at 280 °C was associated

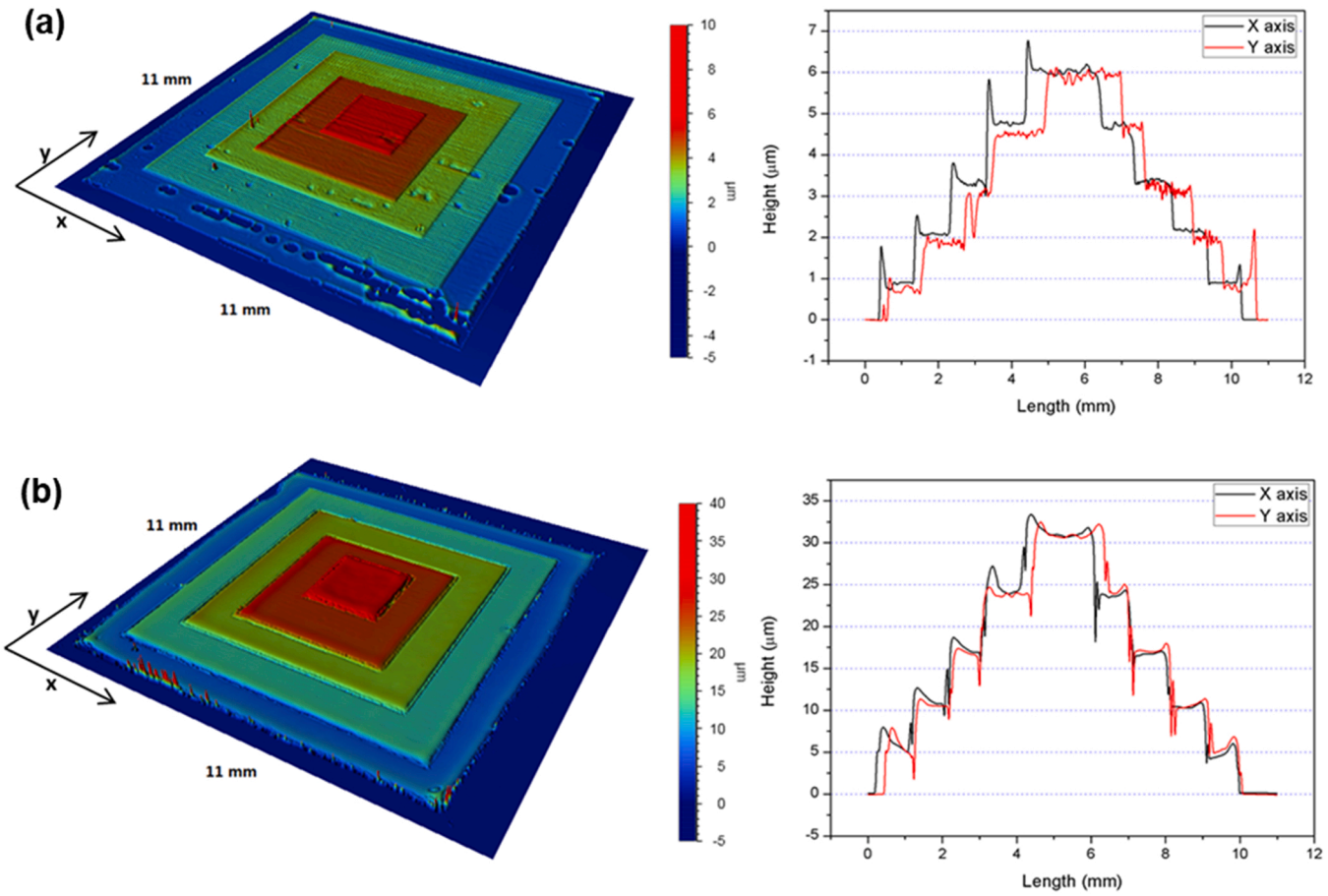

Fig. 6. The surface profile analysis for the 3D ziggurat structure using Bruker Contour GT by the 'polymerisation layer by layer' approach: (a) 1 layer per step; (b) 5 layers per step.

with a weight loss of about 4.0% which was due to the increased viscosity of the PC polymer with the continuous increasing molecular weight. The total weight loss during the melt polymerisation for the dioxane inks sample was about 31.0% which was close to the 32.1% thickness reduction of the films after post curing. Given that the films had a flat top surface and pinned contact lines with the substrate, the reduction of the thickness could be attributed to the by-product formation from the polymerisation. Similarly, for DMF35 printed samples, the weight losses during the 3 isothermal stages also followed a reduced profile, which were 28.8%, 6.2% and 2.7% respectively, subject to the significant increase of polymer viscosity thus suppressed the escape of the methyl salicylate and solvent.

2.3. 3D reactive inkjet printing

To illustrate the capability of 3D printing, a 5-step ziggurat structure was designed, where the bottom layer had a dimension of 10 × 10 mm with a uniform decrement to the top layer of 2 × 2 mm as shown in Fig. 5(a). There was either 1 or 5 consecutive layers printed in each step to determine the effect of the step height on the profile. The structure was created in a 'polymerisation layer by layer' approach where each step was post cured before the following step was printed. DOX25 was attempted due to higher surface flatness and less swelling compared to DMF35 to demonstrate the 3D printing capability. Fig. 5(b) shows a printed ziggurat structure with 5 layers per step. The structures clearly demonstrated optical transparency that other AM processes cannot readily achieve, such as FDM. This also indicated an amorphous structure of the BPA-PC fabricated by this method.

The surface profile analysis results for the ziggurat structures are shown in Fig. 6. The boundaries and heights of each step were clearly distinguished as each step could be built on the previous step which was fully cured after polymerisation in the vacuum oven. The results could be used to determine the step height and the surface uniformity therefore to evaluate the topographic feature of the structure printed by the method. For example, the ziggurat which had 1 layer printed for each step had a flatter feature in the X direction (printing direction) while the Y direction showed a waviness as shown in Fig. 6(a). The cause for this different variation in X and Y directions was that no sufficient reactive mixture in a one single layer would be able to spread over to have the uniform distribution. It was also noted that the bottom step had pinholes which was due to the repeated post processing (e.g., 5 times) that caused depinning during the molten state. The pinhole formation was also likely to be facilitated by the escape of methyl salicylate from the thin layer and the direct heating from the substrate. However, the layers beyond the bottom showed less pinhole formations due to the surface tension (e.g., less de-pinning effect) and possibly a descending temperature gradient to the top that alleviate the defects. As for the ziggurat that had 5 layers per step as shown in Fig. 6(b), the surface showed more flat and uniform topography across X and Y directions for each step. No significant de-pinning phenomenon was seen on the surface, but the edge of the bottom step receded due to the surface tension effect. The substrate temperature had a limited role in influencing the morphologies between the bottom and top steps, as 5 layers on a step had a sufficient material to achieve a uniform coverage. The surface profile of the ziggurat showed an increased step height from the bottom to the top step. For example, the step height increased from approximately 0.8 μm at the bottom step to 1.4 μm at the top step for the ziggurat structure with 1 layer per step; while the ziggurat with 5 layers per step had a step height in the range of 5–7 μm. The main cause of this was likely to be the repeated post processing which led to volume reduction and collapse due to volatilisation of the solvent and the by-product.

While this printing approach showed a promising process design for the direct fabrication of BPA-PC structures, it inherited some limitations from the nature of the materials. Firstly, the reaction between BPA and BMSC followed a polycondensation type, also known as step growth polymerisation, that the molecular weight increase is exponential to the overall conversion of the starting monomers. It led to a slow initial reaction rate that required a lengthy post curing process to achieve a desired molecular weight, compared to some other AM processes such as stereolithography where the monomers would almost crosslink within a few seconds by free radical polymerisation. Secondly, the printing throughput heavily relied on increasing the loading of the reactive mixture in the solvent system to increase the layer thickness. The high percentage of solvent could allow more material spreading which limited the height build up, although it was critical to maintain the printability of the inks with a low viscosity. Thirdly, there would be a maximum layer height that retained a flat top morphology for the next layer to be printed before post curing. Further investigations are suggested to establish a correlation between the surface morphology and the curing time. However, the 'dome' shaped structures could also find some potential applications such as micro-optical devices with a designated optical path.

Table 3
Molecular weight and Đ of different reactive formulations compared to reference PC materials produced from bulk polymerisation by GPC. The cast samples indicated the properties of the original reactive mixtures in the solvent, which were produced by pipetting the reactive inks droplets onto a 10 × 10 × 0.1 mm stainless steel recessed plate and then evaporating the solvent without heating for 2 days. "Low" and "high" refer to two grades of reference BPA-PC provided by SABIC Innovative Plastics lP B.V. as benchmark.

	Cast ($M_w/M_n/Đ$)	As-printed ($M_w/M_n/Đ$)	Post-cured ($M_w/M_n/Đ$)
DOX25	550/500/1.10	650/550/1.18	53200/27800/1.91
DMF35	1100/950/1.16	2600/1900/1.37	29700/17400/1.71
Low PC	N/A	N/A	20700/14400/1.44
High PC	N/A	N/A	30700/20800/1.48

Table 4
1H NMR data assignment for cast, as-printed and post-cured BPA-PC, CDCl3, 300 MHz.

ID	Assigned H	δ H (ppm)
a	CH_3 (3H)	1.70
b	CH (1H)	7.28
c	CH (1H)	7.18
d	CH_3 (3H)	3.95
e(DOX25)	CH_2 (2H)	3.73
e(DMF35)	CH (1H)	8.04
f	CH_3 (3H)	2.98

2.4. Characterisation

A series of as-printed reactive mixtures and post-cured multi-layers samples were characterised and benchmarked to traditionally manufactured BPA-PC samples in terms of molecular weight. The weight-average molecular weight (Mw), number-average molecular weight (Mn) and its polydispersity index Đ (PDI) are summarized in Table 3. The molecular weight of cast samples was measured to demonstrate the printing temperature effect on the initial oligomerisation of the reactive mixture. For DOX25, which indicated a low degree of oligomerisation before printing, and the as-printed sample did not show a significant increase of molecular weight which suggested the ink temperature (60 °C) did not evidently facilitate oligomerisation in the process window. In addition, the molecular weight of DMF35 showed a limited increase from 1100/950–2600/1900 when depositing the reactive mixture onto the 80 °C substrate, which implied a limited effect of the substrate temperature on oligomerisation of reactive mixtures. However, the molecular weight of both ink formulations had a significant growth after thermal post curing. Although Đ of printed samples was higher than that of the reference samples which indicated a broader distribution of molecular chains of post-cured samples, the degree of polymerisation was suggested comparable to those manufactured by

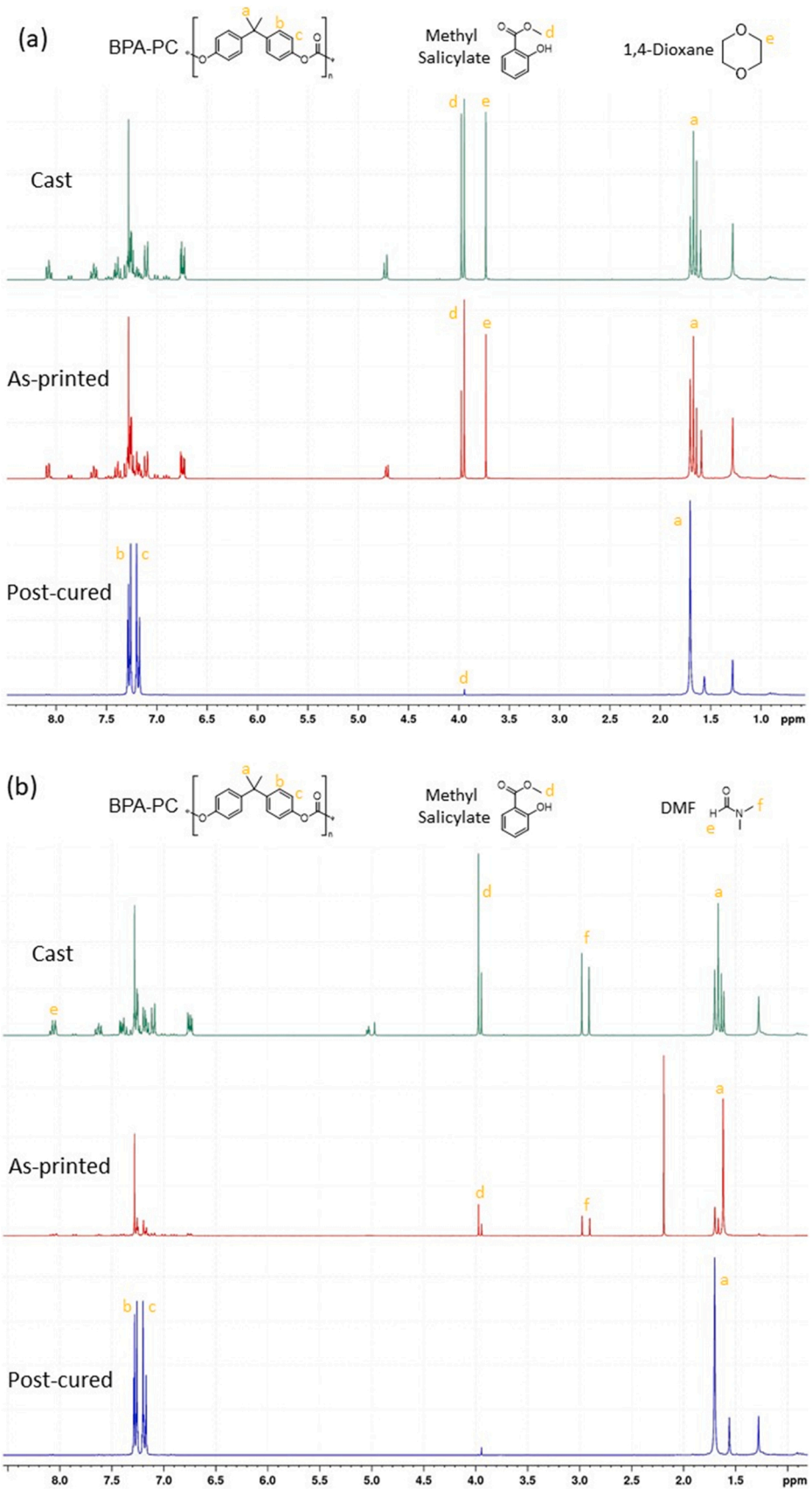

Fig. 7. The ^{1}H NMR spectra for the samples dissolved in $CDCl_3$ at 40 °C: (a) DOX25; (b)DMF35.

Table 5
The T_g values of BPA-PC samples from the DSC thermograms.

	DOX25-PC	DMF35-PC	High M_w PC	Low M_w PC
T_g (°C)	144	141	151	149

Table 6
The thermal data obtained from TGA characterisations. T_0 is the onset of degradation, and recorded as the temperature at which the sample had 1 wt% loss. $T_{5\%}$ is the temperature at which the sample had 5 wt% loss. T_{max} is the temperature at which the sample had the maximum rate of weight loss. Y_c is the yield of char residue.

Sample	Heating rate (°C/min)	T_0 (°C)	$T_{5\%}$ (°C)	T_{max} (°C)	Peak rate (%/min)	Y_c (%)
DOX25-PC	40	416	464	511	1.35	18.8
	20	373	432	490	1.22	17.7
	10	371	422	481	1.30	17.4
DMF35-PC	40	424	469	522	1.25	19.4
	20	377	446	513	1.34	18.6
	10	383	436	497	1.38	18.6
High M_w PC	40	489	521	554	1.93	24.3
	20	469	505	539	1.49	24.9
	10	445	489	525	1.55	24.3
Low M_w PC	40	470	522	559	1.46	24.8
	20	456	497	539	1.60	25.1
	10	443	484	523	1.70	23.6

traditional methods. Also it was noted that post-cured DOX25 had a much higher molecular weight profile than that of DMF35, which was possibly explained by the effect of solvent polarity on a trans-esterification polymerisation [37,38].

The formation of BPA-PC by post thermal curing was confirmed by ^{1}H NMR and ^{13}C NMR. Typical ^{1}H NMR data assignment is shown in Table 4, and its spectra are shown in Fig. 7. There was minor alteration of the chemical shifts between the cast and the as-printed samples, which was in a good agreement with the GPC results where the substrate temperature did not contribute significantly to the oligomerisation. The successful polymerisation of as-printed samples towards BPA-PC was confirmed by the observation of the peak (*a*) intensity increase at 1.70 ppm which was assigned to the protons on the methyl group at the repeating unit of BPA-PC, as well as the intensification at 7.18 and 7.28 ppm (signal *b* and *c*). In addition, the existence of the peak at 3.95 ppm (signal *d*) was attributed to the protons of the methyl group on methyl salicylate, suggesting polymerisation occurred even before the post-curing stage. The significant attenuation of *d* in the polymerised samples indicated the volatilisation of methyl salicylate at the elevated temperature. The ^{13}C NMR spectra (Table S2, Fig. S11, Supplementary Information) also proved the synthesis of BPA-PC from the post-curing stage, which showed the appearance of the carbonate group signal at 148.96 ppm, and the signals at 120.34 and 127.94 ppm assigned to the unsubstituted aromatic carbons [39].

For the appearance of the peak at 3.73 ppm (i.e. the signal *e* which is the protons in –CH_2 on 1, 4-dioxane, as seen in Fig. 7(a)) in the cast and as-printed samples implied that there was solvent residue. There could also be residual solvent in the deposited reactive mixture due to a limited mass transfer rate, that was removed by post curing as the solvent peak disappeared in the polymerised samples. Similarly, the evaporation of DMF was not complete (i.e. the signal *e* of the proton of –CH at 8.04 ppm, and the doublet signal *f* of protons of *trans*- and *cis*-methyl groups at 2.98 and 2.91 ppm, as seen in Fig. 7(b)) until polymerised in the elevated temperature and vacuum environment.

To evaluate the thermal properties of post cured BPA-PC samples, thermal characterisation was carried out by DSC to obtain T_g values which are summarised in Table 5. Although the M_w of DOX25-PC was higher than the reference high M_w PC as previously shown in the GPC results, the measured T_g by this method was not accordingly higher which might indicate that the T_g measurement was affected by the microstructure of the samples (i.e. the granular reference PC samples) [40]. It was still evident that the T_g of post-cured PC samples by the inkjet method was close to the reference PC samples, suggesting a comparable service temperature range with those made by traditional methods. The glass transition observed strongly indicated the amorphous structures of the BPA-PC formed, which helps explain the optical clarity shown in the ziggurat structures printed. Typical DSC thermograms of BPA-PC can be found in Fig. S12 (Supplementary Information).

The thermal stability of BPA-PC was studied by TGA to understand its degradation characteristics at elevated temperature by the method described (Experimental Section, Supplementary Information)). The thermal data obtained from TG and DTG curves were summarised in Table 6. Among the BPA-PC samples made from the two reactive inks at 40°C/min heating rate, T_0, $T_{5\%}$ and T_{max} of DMF35-PC were slightly higher than those of DOX25-PC by 5–11°C. The similar difference of the degradation temperatures was also observed at the heating rate of 20°C/min and 10°C/min. However, the difference was likely to be subject to the higher heat transfer across the samples of the porous surface DMF35-PC which were observed due to the more aggressive escape of methyl salicylate. The two grades of the reference PC samples showed similar thermal degradation characteristics compared to other commercial PC samples [41,42] and significantly higher T_0, T_{max} and Y_c than those of reactive printed PC samples, as shown in Table 6. This characterisation approach suggested that the PC made from 3DIJP could be further studied and optimised in regard to its thermal tolerance.

3. Conclusions

In this paper, a method for fabricating BPA-PC by 3DRIJP has been demonstrated for the first time.

Two representative solvent-based reactive inks (DOX25, DMF35) were formulated using the reactive mixture (BPA, BMSC and TMAH) and two different solvents (1, 4-dioxane, DMF), respectively. The printability of both formulations was assessed, and the printing process windows (ink temperature, substrate temperature and drop spacing) were optimised to print single layer and multi-layer films.

The post curing process was explored in a multi-step heating environment up to 270°C under vacuum to facilitate the molecular chain growth. The surface metrology of the post-cured films was studied, and it was found out DOX25 was suitable for building multi layers due to its flat surface potential. A 3D stepped ziggurat structure using DOX25 was printed with either 1 or 5 layers per step and it was post cured after printing of each step. The surface profile analysis showed a layer flatness and a distinguishable stepped feature of the structure, which demonstrated the capability of the 3DRIJP of BPA-PC. The GPC characterisations of the post-cured samples showed a comparable molecular weight to the commercial reference BPA-PC samples. The 1 H NMR and 13 C NMR spectra confirmed the formation of the BPA-PC with the post-curing method. The DSC study showed the similar glass transition temperatures of the post-processed BPA-PC product with the commercial ones. The TGA results showed the thermal degradation temperature of the post-processed BPA-PC was lower than the commercial samples.

Overall, the significance of this 3DRIJP work was highlighted by the use of a single formulation with a single print head to print reactive monomers, and to polymerise to produce BPA-PC which was difficult to be processed by other AM processes to achieve micron sized features. It broadened the material options for AM and offered novel ideas of processing engineering polymers.

CRediT authorship contribution statement

Hague Richard: Supervision, Writing – review & editing. **Begines Belen:** Investigation, Supervision. **Tuck Christopher:** Funding acquisition, Project administration, Supervision, Writing – original draft, Writing – review & editing. **Kamps Jan Henk:** Resources, Writing –

review & editing. **Price Brian:** Resources, Writing – review & editing. **Gu Hao:** Resources, Writing – original draft. **Wildman Ricky:** Supervision, Writing – review & editing. **Qian Qifeng:** Investigation, Writing – original draft.

Declaration of Competing Interest

The authors declare that they have no known competing financial interests or personal relationships that could have appeared to influence the work reported in this paper.

Acknowledgement

This work was co-funded by the Engineering and Physical Sciences Research Council (EPSRC grant number EP/I033335/2) and SABIC Innovative Plastics BV (Bergen op Zoom, the Netherlands). The authors acknowledged access to facilities and resources of the Centre for Additive Manufacturing at the University of Nottingham. The access to the Department of Chemistry at the University of Nottingham for the use of GPC and NMR facilities supported from Mr Shazad Aslam and Dr Guping He is also gratefully acknowledged.

Appendix A. Supporting information

Supplementary data associated with this article can be found in the online version at doi:10.1016/j.addma.2022.102745.

References

[1] T.J. Horn, O.L.A. Harrysson, Overview of current additive manufacturing technologies and selected applications, Sci. Prog. 95 (2012) 255–282, https://doi.org/10.3184/003685012×13420984463047.
[2] T.D. Ngo, A. Kashani, G. Imbalzano, K.T.Q. Nguyen, D. Hui, Additive manufacturing (3D printing): a review of materials, methods, applications and challenges, Compos. Part B Eng. 143 (2018) 172–196, https://doi.org/10.1016/j.compositesb.2018.02.012.
[3] S.H. Huang, P. Liu, A. Mokasdar, L. Hou, Additive manufacturing and its societal impact: a literature review, Int. J. Adv. Manuf. Technol. 67 (2013) 1191–1203, https://doi.org/10.1007/s00170-012-4558-5.
[4] K.V. Wong, A. Hernandez, A review of additive manufacturing, ISRN Mech. Eng. 2012 (2012) 1–10, https://doi.org/10.5402/2012/208760.
[5] D. Dimitrov, K. Schreve, N. De Beer, Advances in Three Dimensional Printing - state of the art and future perspectives, J. N. Gener. Sci. 4 (2006) 21–49. ⟨http://reference.sabinet.co.za/webx/access/electronic_journals/newgen/newgen_v4_n1_a3.pdf⟩.
[6] M. Vaezi, H. Seitz, S. Yang, A review on 3D micro-additive manufacturing technologies, Int. J. Adv. Manuf. Technol. 67 (2012) 1721–1754, https://doi.org/10.1007/s00170-012-4605-2.
[7] M. Javaid, A. Haleem, Additive manufacturing applications in medical cases: a literature based review, Alex. J. Med. 54 (2018) 411–422, https://doi.org/10.1016/j.ajme.2017.09.003.
[8] H.C.H. Ho, W.L. Cheung, I. Gibson, Morphology and properties of selective laser sintered bisphenol a polycarbonate, Ind. Eng. Chem. Res. 42 (2003) 1850–1862, https://doi.org/10.1021/ie0206352.
[9] K. Thrimurthulu, P.M. Pandey, N.Venkata Reddy, Optimum part deposition orientation in fused deposition modeling, Int. J. Mach. Tools Manuf. 44 (2004) 585–594, https://doi.org/10.1016/j.ijmachtools.2003.12.004.
[10] R.K. Sahu, S.S. Mahapatra, A.K. Sood, A study on dimensional accuracy of fused deposition modeling (FDM) processed parts using fuzzy logic, J. Manuf. Sci. Prod. 13 (2013), https://doi.org/10.1515/jmsp-2013-0010.
[11] W.C. Smith, R.W. Dean, Structural characteristics of fused deposition modeling polycarbonate material, Polym. Test. 32 (2013) 1306–1312, https://doi.org/10.1016/j.polymertesting.2013.07.014.
[12] J. Go, S.N. Schiffres, A.G. Stevens, A.J. Hart, Rate limits of additive manufacturing by fused filament fabrication and guidelines for high-throughput system design, Addit. Manuf. 16 (2017) 1–11, https://doi.org/10.1016/j.addma.2017.03.007.
[13] A. Teichler, R. Eckardt, C. Friebe, J. Perelaer, U. Schubert, Film formation properties of inkjet printed poly(phenylene-ethynylene)-poly(phenylene-vinylene) s, Thin Solid Films 519 (2011) 3695–3702, https://doi.org/10.1016/j.tsf.2011.01.274.
[14] J. Vaithilingam, M. Simonelli, E. Saleh, N. Senin, R.D. Wildman, R.J.M. Hague, R. K. Leach, C.J. Tuck, Combined Inkjet Printing and infrared sintering of silver nanoparticles using a Swathe-by-Swathe and layer-by-layer approach for 3-dimensional structures, ACS Appl. Mater. Interfaces 9 (2017) 6560–6570, https://doi.org/10.1021/acsami.6b14787.
[15] B. Begines, A. Alcudia, R. Aguilera-Velazquez, G. Martinez, Y. He, G.F. Trindade, R. Wildman, M.-J. Sayagues, A. Jimenez-Ruiz, R. Prado-Gotor, Design of highly stabilized nanocomposite inks based on biodegradable polymer-matrix and gold nanoparticles for Inkjet Printing, Sci. Rep. 9 (2019) 16097, https://doi.org/10.1038/s41598-019-52314-2.
[16] N. Reis, C. Ainsley, B. Derby, Viscosity and acoustic behavior of ceramic suspensions optimized for phase-change Ink-Jet Printing, J. Am. Ceram. Soc. 88 (2005) 802–808, https://doi.org/10.1111/j.1551-2916.2005.00138.x.
[17] E.A. Clark, M.R. Alexander, D.J. Irvine, C.J. Roberts, M.J. Wallace, S. Sharpe, J. Yoo, R.J.M. Hague, C.J. Tuck, R.D. Wildman, 3D printing of tablets using inkjet with UV photoinitiation, Int. J. Pharm. 529 (2017) 523–530, https://doi.org/10.1016/j.ijpharm.2017.06.085.
[18] B. Begines, A.L. Hook, M.R. Alexander, C.J. Tuck, R.D. Wildman, Development, printability and post-curing studies of formulations of materials resistant to microbial attachment for use in inkjet based 3D printing, Rapid Prototyp. J. 22 (2016) 835–841, https://doi.org/10.1108/RPJ-11-2015-0175.
[19] Z. Zhou, L. Ruiz Cantu, X. Chen, M.R. Alexander, C.J. Roberts, R. Hague, C. Tuck, D. Irvine, R. Wildman, High-throughput characterization of fluid properties to predict droplet ejection for three-dimensional inkjet printing formulations, Addit. Manuf. 29 (2019), 100792, https://doi.org/10.1016/j.addma.2019.100792.
[20] P.J. Smith, A. Morrin, Reactive inkjet printing, J. Mater. Chem. 22 (2012) 10965, https://doi.org/10.1039/c2jm30649b.
[21] C. Sturgess, C.J. Tuck, I.A. Ashcroft, R.D. Wildman, 3D reactive inkjet printing of polydimethylsiloxane, J. Mater. Chem. C 5 (2017) 9733–9743, https://doi.org/10.1039/C7TC02412F.
[22] R. Zhang, A. Liberski, F. Khan, J.J. Diaz-Mochon, M. Bradley, Inkjet fabrication of hydrogel microarrays using in situ nanolitre-scale polymerisation. Chem. Commun. (2008) 1317–1319, https://doi.org/10.1039/b717932d.
[23] P. Kröber, J.T. Delaney, J. Perelaer, U.S. Schubert, Reactive inkjet printing of polyurethanes, J. Mater. Chem. 19 (2009) 5234, https://doi.org/10.1039/b823135d.
[24] S. Fathi, Fundamental Investigation on Inkjet Printing of Reactive Nylon Materials, University of Loughborough, 2011 (Accessed January 12, 2015), ⟨https://dspace.lboro.ac.uk/dspace-jspui/handle/2134/7832⟩.
[25] J. Akola, R.O. Jones, Branching reactions in polycarbonate: a density functional study, Macromolecules 36 (2003) 1355–1360, https://doi.org/10.1021/ma021630j.
[26] J.H. Kamps, R. Groote, M. Baus, H. Vermeulen, T. Hoeks, R. van der Heijden, R. P. Sijbesma, J.P.A. Heuts, Activated carbonates: enabling the synthesis of differentiated polymers via solution carbonation, Eur. Polym. J. 135 (2020), 109901, https://doi.org/10.1016/j.eurpolymj.2020.109901.
[27] J.H. Kamps, T. Hoeks, E. Kung, J.P. Lens, P.J. McCloskey, B.A.J. Noordover, J.P. A. Heuts, Activated carbonates: enabling the synthesis of differentiated polycarbonate resins via melt transcarbonation, Polym. Chem. 7 (2016) 5294–5303, https://doi.org/10.1039/C6PY00925E.
[28] J.H. Kamps, V. Ramakrishnan, T. Hoeks, B.J.P. Jansen, R.P. Sijbesma, J.P.A. Heuts, Microphase separation: enabling isosorbide-based polycarbonates with improved property profile, Macromolecules 52 (2019) 3187–3198, https://doi.org/10.1021/acs.macromol.8b02546.
[29] A. Aerts, C. Kroonen, J.H. Kamps, R.P. Sijbesma, J.P.A. Heuts, High molar mass polycarbonate via dynamic solution transcarbonation using bis(methyl salicyl) carbonate, an activated carbonate, Macromol. Chem. Phys. 222 (2021), 2100186, https://doi.org/10.1002/macp.202100186.
[30] B. Derby, Inkjet printing of functional and structural materials: fluid property requirements, feature stability, and resolution, Annu. Rev. Mater. Res. 40 (2010) 395–414, https://doi.org/10.1146/annurev-matsci-070909-104502.
[31] N. Reis, C. Ainsley, B. Derby, Ink-jet delivery of particle suspensions by piezoelectric droplet ejectors, J. Appl. Phys. 97 (2005), 094903, https://doi.org/10.1063/1.1888026.
[32] D. Soltman, V. Subramanian, Inkjet-printed line morphologies and temperature control of the coffee ring effect, Langmuir 24 (2008) 2224–2231, https://doi.org/10.1021/la7026847.
[33] T. Kajiya, M. Doi, Dynamics of drying process of polymer solution droplets: analysis of polymer transport and control of film profiles, J. Soc. Rheol. Jpn. 39 (2011) 17–28, https://doi.org/10.1678/rheology.39.17.
[34] S.H. Lee, Y.J. Cho, Characterization of silver inkjet overlap-printing through cohesion and adhesion, J. Electr. Eng. Technol. 7 (2012) 91–96, https://doi.org/10.5370/JEET.2012.7.1.91.
[35] J. Stringer, B. Derby, Formation and stability of lines produced by inkjet printing, Langmuir 26 (2010) 10365–10372, https://doi.org/10.1021/la101296e.
[36] C. Sturgess, C. Tuck, I.A. Ashcroft, R.D. Wildman, 3D reactive inkjet printing of polydimethylsiloxane, J. Mater. Chem. C 5 (2017) 9733–9743, https://doi.org/10.1039/C7TC02412F.
[37] J.-P. Hsu, J.-J. Wong, Kinetic modeling of melt transesterification of diphenyl carbonate and bisphenol-A, Polymer 44 (2003) 5851–5857, https://doi.org/10.1016/S0032-3861(03)00605-0.
[38] R. Nishihara, The novel process for diphenyl carbonate and polycarbonate production, Catal. Surv. Asia 14 (2010) 140–145, https://doi.org/10.1007/s10563-010-9095-3.
[39] M. Goyal, R. Nagahata, J. Sugiyama, Michihiko Asai, M. Ueda, K. Takeuchi, Direct synthesis of aromatic polycarbonate from polymerization of bisphenol A with CO using a Pd–Cu catalyst system, Polymer 40 (1999) 3237–3241, https://doi.org/10.1016/S0032-3861(98)00579-5.

[40] S.D. Thorat, P.J. Phillips, V. Semenov, A. Gakh, Physical properties of aliphatic polycarbonates made from CO_2 and epoxides, J. Appl. Polym. Sci. 89 (2003) 1163–1176, https://doi.org/10.1002/app.12355.
[41] B.N. Jang, C.A. Wilkie, A TGA/FTIR and mass spectral study on the thermal degradation of bisphenol A polycarbonate, Polym. Degrad. Stab. 86 (2004) 419–430, https://doi.org/10.1016/J.POLYMDEGRADSTAB.2004.05.009.
[42] S. Liu, H. Ye, Y. Zhou, J. He, Z. Jiang, J. Zhao, X. Huang, Study on flame-retardant mechanism of polycarbonate containing sulfonate-silsesquioxane-fluoro retardants by TGA and FTIR, Polym. Degrad. Stab. 91 (2006) 1808–1814, https://doi.org/10.1016/J.POLYMDEGRADSTAB.2005.11.013.